CO$_2$ Gas Barrier Properties in Polymer Nanocomposite Coatings Containing Li-Hectorite Clays

Georgios A. Choudalakis,[1] Hussein Kalo,[2] Josef Breu,[2] Alexandros D. Gotsis[1]

[1]Department of Sciences, Technical University of Crete, GR-73100 Hania, Greece
[2]Department of Chemistry, University of Bayreuth, D-95447 Bayreuth, Germany
Correspondence to: G. A. Choudalakis (E-mail: gchoudalakis@isc.tuc.gr)

ABSTRACT: This is a study of the addition of hydrophilic Li-hectorite nanoplatelets in waterborne acrylic resin emulsions and the resulting nanocomposite coatings. The mechanism of the dispersion of the nanoplatelets during film formation and curing from aqueous suspensions is described. The morphological features of the coating and the state of delamination is examined via X-ray diffraction for three different clay treatment procedures. The influence of the shape of the nanosized objects and their dispersion level on the transport characteristics of the nanocomposite film are measured and their effect on the polymer free volume is discussed. © 2014 Wiley Periodicals, Inc. J. Appl. Polym. Sci. **2014**, *131*, 40805.

INTRODUCTION

To improve the mechanical and barrier properties of a coating, inorganic phyllosilicate reinforcement may be dispersed in the matrix.[1–4] When the particles have nanosized dimensions, the desired properties are usually reached in the coating at low filler volume fractions. The coating retains, thus, its macroscopic homogeneity and low density. The large effect of the nanoparticles is due to the huge internal surface area ($\sim$750 m^2/g) that is generated, as the character of the matrix material in these interfacial regions dominates the bulk.

Waterborne nanocoatings are formulations that have water as main carrier and are reinforced with particles of nanodimensions.[1] These coatings, thus, avoid the organic solvents. The most common inorganic particle reinforcements in nanocoatings are the smectite clays. In their natural state, the clay consists of crystalline silicate layers stacked on top of each other. The individual layer thickness is around 1 nm, and its lateral dimensions vary from 30 nm to several μm, i.e., nominal *L/D* values of 50–1000 or higher. The inter-layer gaps (10–15 Å) are called galleries.

The large surfaces of the clay follicles are electrically charged. The negative charge is compensated by the presence of cations in the galleries and the stacks are stabilized. When suspended in water, the water molecules penetrate the inter-layer region of the smectite and hydrate the exchangeable cations.[5] The resulting repulsive hydration forces lead to separation of the layers by 10–20 Å (crystalline swelling).

The expansion of the inter-layer distance weakens the attractive forces between the crystalline layers. When ultrasonic waves hit the suspension, the expanded particulates absorb the ultrasonic energy, which is used for the separation of the individual crystalline layers. The reaggregation of the delaminated particles in the water or any other liquid of high dielectric constant is prevented by the development of long range repulsive forces, which prevail over the attractive van der Waals forces.[6] By mixing this finely dispersed suspension with a water-borne resin emulsion, extracting the water (drying) and curing the resin, an exfoliated nanocoating can be obtained. Thus, the use of waterborne resins seems to be the most efficient way to manufacture nanoplatelet reinforced coatings with well exfoliated clays.

Polymers are mostly incompatible to inorganic particles and produce composites with aggregated nanoparticles. Even when there is some compatibility, the simple mixing of polymer and layered silicates does not always result in a nanocomposite. Various factors, such as clay volume fraction, large surface areas, molecular weight of the monomers, radius of gyration of the polymer, strength of the interactions between the different phases etc. are of importance and affect the degree of wettability of the clay layer surfaces by the polymer molecules.[7]

Further, the extensive surface area of the inorganic layers requires more and/or larger resin monomers to become saturated and to prevent reagglomeration. If the radius of gyration, R_g, of the polymer coil is much smaller than the lateral dimension, *L*, of the layer, many macromolecules are required to
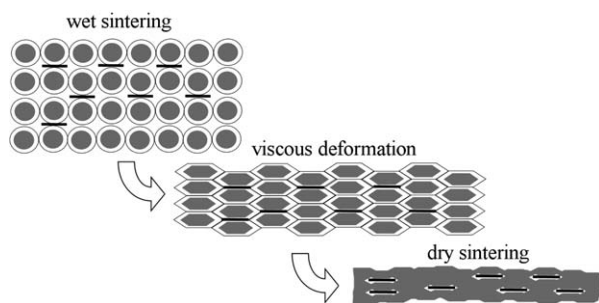
Figure 1. Representation of the nanocomposite coating formation process.

saturate these surfaces. Thus, for relatively high volume fractions of clay, an attractive force may be developed between the platelets, which induces phase separation. Consequently, in many polymer–clay nanocomposites systems, such as in waterborne resins, the maximum dispersible volume fraction of the clay, usually does not exceed 10 vol %.

During drying and curing of the nanocomposite, various overlapping physical and chemical processes take place.[8] Initially, the evaporation of the water leads to a close-packed arrangement of resin droplets and exfoliated nanoparticles. In this stage, which is referred to as wet sintering, there is still a residual repulsive barrier that acts against coagulation. When the ionic strength, which is related to the Debye length, reaches the critical coagulation concentration, due to the evaporation of the water, the screened electrostatic repulsions can no longer overcome the van der Waals attraction. The droplets will start, then, to deform, due to the capillary pressure across the water/air menisci, closing the existing pores. Then, the monomers will inter-diffuse across the droplet boundaries and the droplets coalesce. The final stage in the formation of the coating is the initiation of the crosslinking reactions, which is referred as dry sintering.

The kinetics of the film formation is determined by the rates of the various processes above. The water (solvent) evaporation rate depends on the temperature and the humidity of the surrounding air. The particle aggregation rate depends mainly on the volume fraction, since it is determined by the face-to-face distance of the nanolayers. The crosslinking reaction rate depends on the temperature and the chemical nature of the reactants. The rate of diffusion of the reactants is determined by the thermodynamics and the free volume.[8]

When the evaporation rate is faster than the particles diffusion rate, any rearrangement (reaggregation) of the nanoparticles is prevented by the high viscosity and low free volume. This will cause jamming of the nanoparticles, which results in their entrapment in random places. Therefore, the polymer particles create a template on which the dispersed inorganic phase is arranged (Figure 1). Since the kinetics and the thermodynamic state of the system are governed by the Brownian motions of the constituents, the entrapping of the particles will depend mainly on their size and volume fraction. Thus, in dilute systems, where the volume fraction of the particles is relatively low, the entrapping mechanism is expected to be more efficient.

Various models have been proposed for the prediction of the permeability in nanoplatelet reinforced materials.[3,4] Most models are based on the idea that the platelets form a tortuous path for the permeating molecules and assume that the physical properties of the polymer matrix itself are not affected by the presence of the inorganic particles. The tortuosity concept that the models (and some experimental observations[9]) use does not depend on the type of the diffusing gas. The validity and applicability of various permeability models is tested in the present work and ideas for improvement are proposed.

Sun et al.[10] reported a successful preparation of nanocomposites via a simple mixing of clay and polymer latexes in aqueous solutions under ultrasonification. They claimed a significant improvement of the barrier properties against water and water vapor. Dai et al.[11] reported an 86% reduction on oxygen permeability in epoxy resin-organomodified clay nanocomposites prepared by in situ thermal ring-opening polymerization. Recently, Möller et al.[12] managed to disperse 11 vol % of hectorite in UV-curable polyurethane and observed a more than two orders of magnitude reduction of the relative permeability.

This article examines nanocomposites made via a direct mixing of synthetic hydrophilic Li-hectorite particles in a waterborne acrylic resin emulsion. The gas transport coefficients of the resulting coating were measured and correlated with the morphological characteristics of the system. In their exfoliated state, the inorganic nanoparticles have very anisometric dimensions, i.e., aspect ratios (width/thickness ratio). As the impermeable crystalline clay layers create tortuous paths for diffusion inside the matrix (Figure 2), they hinder the transport of gas molecules and reduce the gas permeability of the material.[4] However, the incorporated particles may cause free volume changes in the polymer matrix, especially at the large interfacial regions between the two components, which may limit this reduction or even reverse it.[13] This was the case when low aspect ratio laponite disks were incorporated in the acrylic resin.[14] The redistribution of the free volume hole sizes caused by the particles in combination with the low tortuosity, results destructively on the barrier properties of the nanocoating.

There seems, therefore, that two antagonistic parameters affect the permeability of gasses in the nanocomposite coating. The aspect ratio of the particles is responsible for the tortuosity in the diffusion path, while the interfacial areas can promote
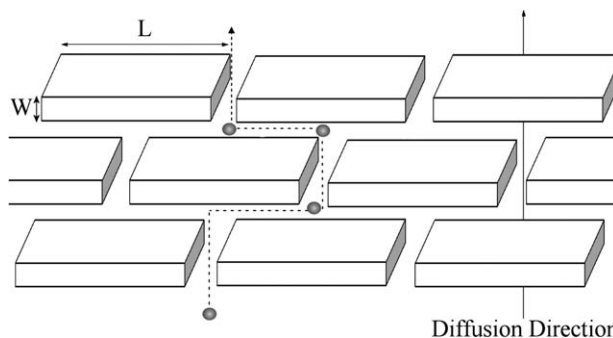
Figure 2. The ideal case of the periodical arrangement of the dispersed clay crystalline layers.

increases in the solubility. In this article we use nanoplatelets with extremely high values for the aspect ratios to examine whether these values can tilt the balance to the desired enhancement of the barrier properties.

The research on the gas barrier performance of polymer–clay nanocomposites concerns mostly water vapor, oxygen, carbon dioxide, and nitrogen[15–18] for packaging, storage, and protection of electronic devices. The objective of this work is the development of an acrylic nanocoating with improved barrier properties for nonpolar gasses, such as carbon dioxide. The use and the potential of the synthetic Li-hectorite as a candidate reinforcing additive in polymeric coatings is shown to have promising perspectives for enhanced barrier performance.

It is found in this work that the incorporation of hydrophilic Li-Hectorite nanoparticles in acrylic resin matrix produces nanocomposite membranes with enhanced gas barrier properties. It seems that the gas permeation process as a function of particles volume fraction can be divided in two regions. Nielsen's model[19] describes the behavior of the relative diffusivity in the dilute region adequately, while Cussler's model[20] is more appropriate to be used in the semidilute region. During the film formation process, a significant amount of free space (excess free volume) can be created, affecting the gas diffusion. The cure of this problem is the complete removal of the solvent during film formation. The gas barrier performance of the Li-hectorite/polymer coatings can become even higher if the exfoliated layers are not allowed to bend and remain flat.

EXPERIMENTAL

Li-Hectorite Clay

Since the thickness of the single clay layers is around 1 nm, only the lateral dimension can be extended to increase their aspect ratio L/W. This is achieved by choosing the appropriate synthesis conditions, such as crystallisation temperature, choice of inter-layer cations, layer surface charge, and composition. Möller et al.[21] synthesized such a Li-Hectorite clay with a very large L dimension by a fast high temperature melt synthesis technique. Details on this production technique can be found in their articles.[21,22] Huge aspect ratios were achieved, of the order of 10,000 or more. It has been claimed that this clay is spontaneously delaminated upon immersion in water and no additional shearing or ultrasonic treatment is needed, due to the large hydration enthalpy of the Li inter-layer cation.[21] This reference also gives the size distribution of the Li-hectorite used here.

Aqueous Clay Suspension

A certain amount of untreated Li-hectorite was added to deionized water (0.01 g/mL). Three different treatment processes were followed: (i) the clay powder was added in the water by simple mixing with no further treatment; (ii) the aqueous clay suspension was sonicated in an ultrasound bath for 30 min; (iii) the suspension was subjected at a high shearing flow for 30 min at 3500 rpm and then was sonicated for 15 min using an ultrasonic probe (400W Hielscher®) operating at 35 kHz. Since the ultrasonic probe is immersed in the sample container, it can deliver much higher energy than the ultrasonic bath (100×). As
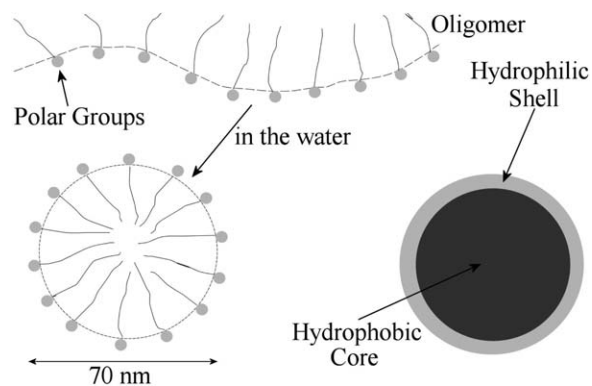
Figure 3. The form of the colloidal resin droplets in the aqueous emulsion.

the ultrasonic energy decreases radially and axially from the probe, the space between the probe and the wall of the container was kept as low as possible.

The transfer of ultrasonic energy in the system is due to the collapsing of the cavitation bubbles. The violently collapsing bubbles create large pressures locally, in the order of 1000 atm. Under these pressures, the primary clay tactoids can be delaminated into individual crystalline layers. In some cases there is even a suspicion of crystalline layer fragmentation. During the ultrasonication, the temperature of the solution increases significantly. This can have two opposites effects: On the one hand, high temperature facilitates the disruption of the attraction forces; on the other hand the evaporation of the solvent is accelerated and its vapor fills the cavitation bubbles, which tend to collapse less violently. In order to compensate these effects, the sample container was placed in a water bath during ultrasonication treatment.

Waterborne Acrylic Resin Emulsion

Setalux 6768 (provided by Nuplex Resins, $\rho = 1.04$ g/cm^3) a speciality acrylic emulsion in water with 40% resin was used for the matrix. This resin is self-crosslinkable, the crosslinking reaction is triggered upon drying and results in a fully cured coating. The droplets of the acrylic resin contain hydrophilic groups. The nonpolar segments of the monomers associate with each other to form colloidal aggregates (droplets), while the polar groups reside on their periphery (Figure 3). These composite droplets are dispersed in the continuous phase (water) and form the resin emulsion. The mean size of each droplet is about 60–70 nm.[1]

The hydrophilic shell of the droplets has a glass transition temperature of about 40°C, while the T_g of the hydrophobic core is about 120°C. The glass transition temperature of the cured resin was measured by DMA[1] to be above 100°C. The minimum film formation temperature T_{MFF} is around 7°C.

Significant droplet deformation can take place if drying occurs at temperatures well above T_{MFF} and a transparent, pore-free polymer film forms then. If the drying temperature is below or close to T_{MFF}, droplet deformation will be incomplete. Although the final film may be transparent then, it is a porous structure

Table I. Characteristics of the Samples Containing Hectorite Nanoparticles

Sample	wt %	Vol %	Density (g/cc)	d (mm)
Resin	0	0	1.040	0.88
Hectorite	100	100	2.600	–
1U	0.84	0.34	1.0453	0.71
2U	1.67	0.67	1.0505	0.69
3U	2.86	1.16	1.0582	0.7
4U	5.5	2.30	1.075	0.72
5U	6.4	2.70	1.082	0.60
6U	9.1	3.85	1.100	0.375
1B	0.84	0.34	1.0453	0.91
2B	1.25	0.50	1.478	1.02
3B	2.17	0.88	1.0537	1.00
1W	0.84	0.34	1.0453	0.914
2W	1.25	0.50	1.0478	0.79
3W	2.10	0.88	1.0537	0.75
4W	3.25	1.33	1.061	0.56

The letter U in the code denotes samples treated with ultrasound, W denotes samples without any treatment and B denotes samples treated in an ultrasound bath.

of individual particles with a network of hydrophilic surfactant material present at the particle–particle interface.

Nanocoatings
The nanocomposites were prepared by mixing the aqueous Li-hectorite nanoparticle dispersions with the aqueous acrylic resin emulsion, letting them dry at 23°C and 50% relative humidity and curing. The curing temperature was well above T_{MFF} but lower than the glass transition temperature of the hydrophilic shell of the droplets.

Since below T_g the free volume in the polymer is reduced, the diffusion rate of the nanoparticles decreases, their mobility is hindered and the possibility for reaggregation is reduced. The curing temperature is critical for various more reasons: It accelerates the reaction rate (dry sintering), reduces the time available for wet sintering and for the viscous deformation of the resin droplets. When the droplets cannot deform completely, the capillary pressure will produce elastic deformation, that stores energy in the droplet packing stage, and cracks may appear in the coating.[23] Additionally, when the solvent evaporation rate becomes very high, the repulsive forces, which stabilize the suspensions, disappear quickly and reaggregation can be accelerated. In other words, when the solvent is rapidly driven off, the resin de-wets the clay, leading to stacked structures. It should be noted that, inevitably, a small amount of solvent remains in the coating after the end of curing. This is because curing starts from the outer surface of the film and continues inwards. A layer of completely deformed particles near the film surface will form a diffusion barrier for the remaining water in the film, sealing off further evaporation.

Several samples were prepared in the form of cured films with various volume fractions of nanoparticles. In order to prepare

samples for the permeation experiments, the nanocomposite dispersions were smeared on sparse glass fiber filters. After hardening, this produced a compact (nonporous) membrane (the nanocomposite) mechanically reinforced by the glass fibers of the filter, of total thickness between 0.4 and 1.0 mm. The sample characteristics are shown in Table I. The average actual thickness, d, of the membranes (the cured coating itself, excluding the substrate) were calculated from the mass of the sample (including the reinforcing filter), m_s, the mass of the filter, m_{flt}, the density ρ_{comp} the nominal area, A, of the sample (directly exposed to the gas):

$$d = \frac{m_s - m_{flt}}{\rho_{comp}} \frac{1}{A} \quad (1)$$

where $\rho_{comp} = \frac{\rho_{part}\rho_{resin}}{w\rho_{resin} + (1-w)\rho_{part}}$ and w is the weight fraction of the particles in the sample.

Measurements
The morphological features of the samples were investigated using X-ray diffraction. The XRD patterns were collected for angles 2θ between 1.5 and 15° using a Rigaku® diffractometer with a CuK$_\alpha$ radiation source of wavelength $\lambda = 1.5406$ Å and a scanning step of 0.02 deg/s. The degree of exfoliation was studied as a function of hectorite particles loading and for three different clay treatment processes.

Gas permeability measurements were performed in a permeation cell. The cell was divided hermetically by the membrane in two compartments. The right compartment contained a CO_2 gas sensor supplied by Vaisala® of Finland. The measuring range of the sensor was 0–5000 ppm of CO_2.

Both chambers of the cell were filled initially with He gas at 1 atm for 24 h. This procedure removed any possible residue of CO_2 that might have been absorbed by the membrane. Then the left chamber was filled with CO_2 at 1 atm and the CO_2 concentration in the right chamber was recorded as a function of time. Using Fick's first law, the concentration of the gas that permeates the membrane at steady state is given by the following relation[4]:
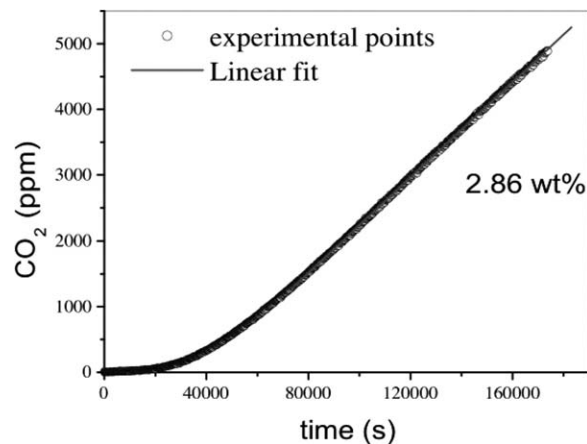
Figure 4. Experimental curve of the concentration of the gas that permeates the membrane as a function of time, measured in a permeation cell, for the sample 3U. Each experimental point originates from the averaging of 10 measurements taken every 10 s.
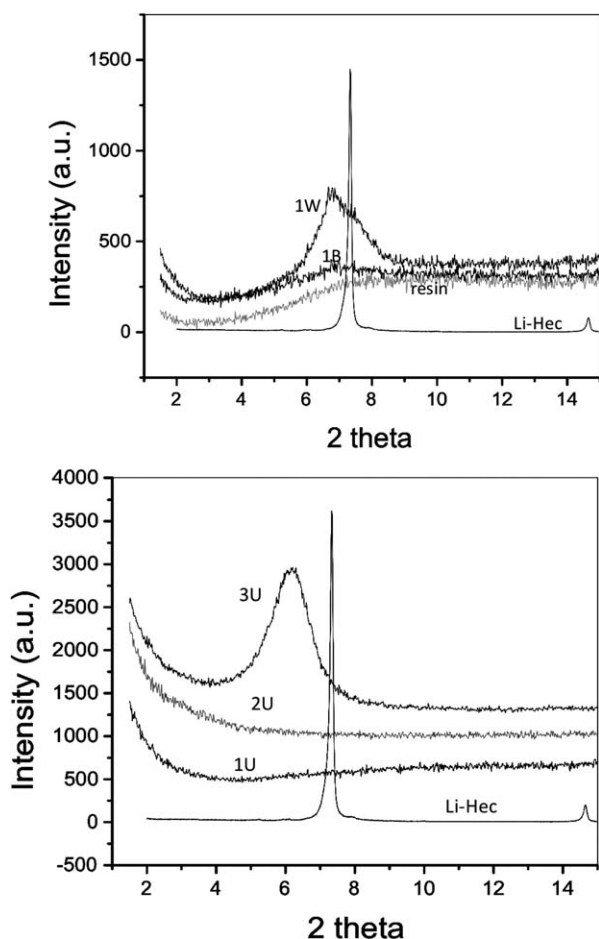
Figure 5. X-ray diffraction patterns of hectorite nanocomposites: (a) 0.34 vol % hectorite sample treated in ultrasound bath (1B); and without ultrasonication (1W). (b) Three samples containing different volume fractions of clay treated with the ultrasonication probe for 15 min.

$$c = \frac{ADSp}{Vd}(t - t_L) \qquad \text{with} \qquad t_L = \frac{d^2}{6D}, \qquad (2)$$

where $A = 23.76$ cm^2, D is the diffusion coefficient, S is the solubility coefficient, p is the initial pressure ($= 1$ atm), V is the volume of the chamber that contains the sensor, d is the membrane thickness and t_L is the time lag to reach steady state.[4] The time lag is determined by extrapolation of the straight portion (which corresponds to steady state) of the $c(t)$ curve to zero concentration (Figure 4). The slope of the curve at steady state gives the permeability coefficient $P = D S$. Thus, the diffusion coefficient, D, can be determined directly by measuring t_L and, then, the solubility, S, can be extracted from the value of P determined from the slope.

Positron annihilation lifetime spectra were recorded at room temperature using ^{22}Na as radioactive positron source. The source was located between two flat pieces of the sample with an appropriate thickness of 2 mm so that the positrons could be stopped in the bulk. Each spectrum contained $\sim 10^6$ counts and was analyzed by the LT® computer program into three components. After the background subtraction and source corrections, the variance of the fit was less than 1.2. More details on the PALS method are given by Pethrick[24]; Choudalakis et al.[14]

RESULTS AND DISCUSSION

X-ray Diffraction

The primary Bragg peak of the Li-hectorite powder appears at $2\theta = 7.3°$ and is narrow and sharp indicating thick tactoids with an inter-layer distance of about 12 Å. The osmotic swelling of the Li-hectorite by water[16] shifts the peak to slightly lower angles, where it remains also in the nanocomposite. This shift, thus, may not be an indication of intercalated morphology. Exfoliated samples do not show any such peak. The nanocomposite samples that had not received any ultrasound treatment show an obvious peak [e.g., sample 1W in Figure 5(a)]. Ultrasonication using a bath reduces this peak [Sample 1B in Figure 5(a)]. Therefore, it seems that the ultrasound treatment has a small effect on the exfoliation state of the clay. This is added to the impact of the large hydration enthalpy of the Li$^+$ inter-layer ion.[17] The effect of the ultrasound bath on the degree of exfoliation of the nanolayers is relatively weak, while an ultrasound immersion probe is much more efficient. At low volume fractions the peak disappears when the sonication probe is used [Samples 1U and 2U in Figure 5(b)] and delamination is expected.

At higher volume fractions the diffraction peak reappears [Sample 3U, Figure 5(b)]. It seems that there is a transition from a dilute to a semidilute system at less than 1 vol % nanoparticles. Since the hectorite crystalline layers have huge lateral dimensions, it is expected that there will be a strong overlapping of the platelets, even for volume fractions below 1%. Please note that, besides delamination, the intensity of the 001 reflection may also be affected by the number of particles within the scatter area of the beam and by random interstratification, something which we have neglected in our discussion for simplicity.

Gas Permeability Models

Nielsen[19] calculated the tortuosity factor τ caused by the impermeable crystalline layers by simple geometrical considerations (Figure 2) to be

$$\tau = 1 + \frac{\alpha\phi}{2}, \qquad (3)$$

where $\alpha = L/W$, and ϕ is the volume fraction of the layers. Therefore, the diffusion coefficient is reduced by the factor τ and the relative diffusivity D_{comp}/D_{matrix} becomes:

$$\frac{D_{comp}}{D_{matrix}} = \frac{1}{1 + \frac{\alpha\phi}{2}}. \qquad (4)$$

Assuming that the incorporation of the nanoparticles does not alter the physical characteristics of the matrix (free volume), the solubility coefficient can be written as:

$$S_{comp} = S_{matrix}(1 - \phi). \qquad (5)$$

Since the permeability coefficient is $P = DS$, the relative permeability becomes:

$$\frac{P_{comp}}{P_{matrix}} = \frac{1 - \phi}{1 + \frac{\alpha\phi}{2}}. \qquad (6)$$

In a more complex geometrical approach, Cussler et al.[20] came to the following model:

Table II. CO_2 Gas Transport Coefficients of the Samples at 23°C and 50% rel. Humidity, Measured in the Permeability Cell

Sample	Volume fraction (%)	Diffusion coeff. 10^{-12} m^2 s^{-1}	Relative diffusion coeff.	Solubility 10^{-5} mol m^{-3} Pa^{-1}	Relative solubility	Permeability 10^{-16} mol m^{-1} s^{-1} Pa^{-1}	Relative perm.
	0	5.15	1.00	6.9	1.00	3.55	1.00
1U	0.34	3.2	0.62	9.4	1.36	3	0.85
2U	0.67	2.67	0.52	9.2	1.33	2.66	0.75
3U	1.16	2.15	0.42	7.7	1.12	1.65	0.46
4U	2.3	1.42	0.28	8.2	1.19	1.17	0.33
5U	2.7	0.8	0.16	7.5	1.09	0.6	0.17
6U	3.85	0.31	0.06	7.2	1.04	0.22	0.06
1B	0.34	3.79	0.74	8	1.16	3.05	0.86
2B	0.5	3.85	0.75	7.2	1.04	2.76	0.78
3B	0.88	3.3	0.64	7.7	1.12	2.52	0.71
1W	0.34	3.8	0.74	8	1.16	3.03	0.85
2W	0.5	3.3	0.64	9.3	1.35	3.07	0.86
3W	0.88	2.7	0.52	8.8	1.28	2.36	0.66
4W	1.33	1.47	0.29	9.1	1.32	1.34	0.38

$$\frac{P_{\text{comp}}}{P_{\text{matrix}}} = \left(1 + \frac{\alpha^2 \phi^2}{1-\phi}\right)^{-1}. \tag{7}$$

This model is based on the assumption of narrow slits, which means that the horizontal distances of the particles are minimum (semidilute system). The relative diffusivity then becomes:

$$\frac{D_{\text{comp}}}{D_{\text{matrix}}} = \frac{1}{1-\phi+\alpha^2\phi^2}. \tag{8}$$

Taking into account the randomness in spatial positioning of parallel platelets, Lape et al.[25] developed a 2D model based on the idea that the tortuosity is due not only to the increased path length but also to the reduced area:

$$\frac{P_{\text{comp}}}{P_{\text{matrix}}} = \frac{1-\phi}{\left(1+\frac{\alpha\phi}{3}\right)^2}. \tag{9}$$

This gives for the relative diffusivity:

$$\frac{D_{\text{comp}}}{D_{\text{matrix}}} = \frac{1}{\left(1+\frac{\alpha\phi}{3}\right)^2}. \tag{10}$$

In a different approach, but using parallel circular disks, Gusev and Lusti[26] developed a 3D model based on the solution of the Laplace equation for the local chemical potential, which gives:

$$\frac{P_{\text{comp}}}{P_{\text{matrix}}} = \exp\left[-\left(\frac{\alpha\phi}{x_0}\right)^{\beta}\right], \tag{11}$$

where $x_0 = 3.47$ and $\beta = 0.71$ are fitting parameters. The relation between the disk aspect ratio ($\alpha_{\text{disk}} = R/W$) and the rectangular platelet aspect ratio ($\alpha_{\text{rect}} = L/W$) of the other models can be derived by comparing the area of a disk, πR^2, to the area a rectangular platelet, L^2.[4] Thus:

$$\alpha_{\text{disk}} = \alpha_{\text{rect}}/\sqrt{\pi} \tag{12}$$

There are also models which take into account the orientation of the particles.[4] However, we limit the interpretation of our

results in parallel particles, since the clay-platelets are probably forced to align on the average in parallel, even in a sparse suspension, due to their high degree of anisometry. The degree of alignment depends strongly on the aspect ratio. The larger the lateral dimensions of the thin platelets, the better the alignment will be in the film. Free rotation is hampered by the large hydrodynamic radii, often resulting in liquid-crystalline ordering and birefringence.[12] In the same line, the continuously increasing concentration of the suspension as the solvent evaporates enhances the alignment of the platelets.

Gas Transport Coefficients

Table II summarizes the mass transport coefficients of the CO_2 gas in the nanocomposite samples. The effect of the ultrasound bath on the diffusivity of the samples is very small, as it can also be seen in Figure 6(a). Fitting Nielsen's equation (eq. 4) gives an aspect ratio for the particles in the order of 140. This is very low compared the nominal lateral dimension of the layer, $L \sim 10,000$ nm. The reduction of D by addition of less than 1 vol % nanoparticles is about 35%.

The solubility coefficient on the other hand, shows an increase of 10% [Figure 6(b)]. This is probably due to the large interfacial regions between the two components. Thus, the permeability coefficient ($P = DS$) is reduced by only 30% at the highest volume fraction. The tortuosity effect seems to dominate over the possible free volume enhancement. This shows that the estimation of the aspect ratio by fitting only the permeability coefficient data in Nielsen's model is not always accurate. Better predictions can be made when all three transport coefficients are known.

In the case of the samples that have not been treated by ultrasonication the degree of delamination of the particles is somewhat lower. The tortuosity effect exists, then, but the solubility is enhanced significantly [Figure 6(b)]. Even in this case, however, an almost linear reduction of the relative permeability is
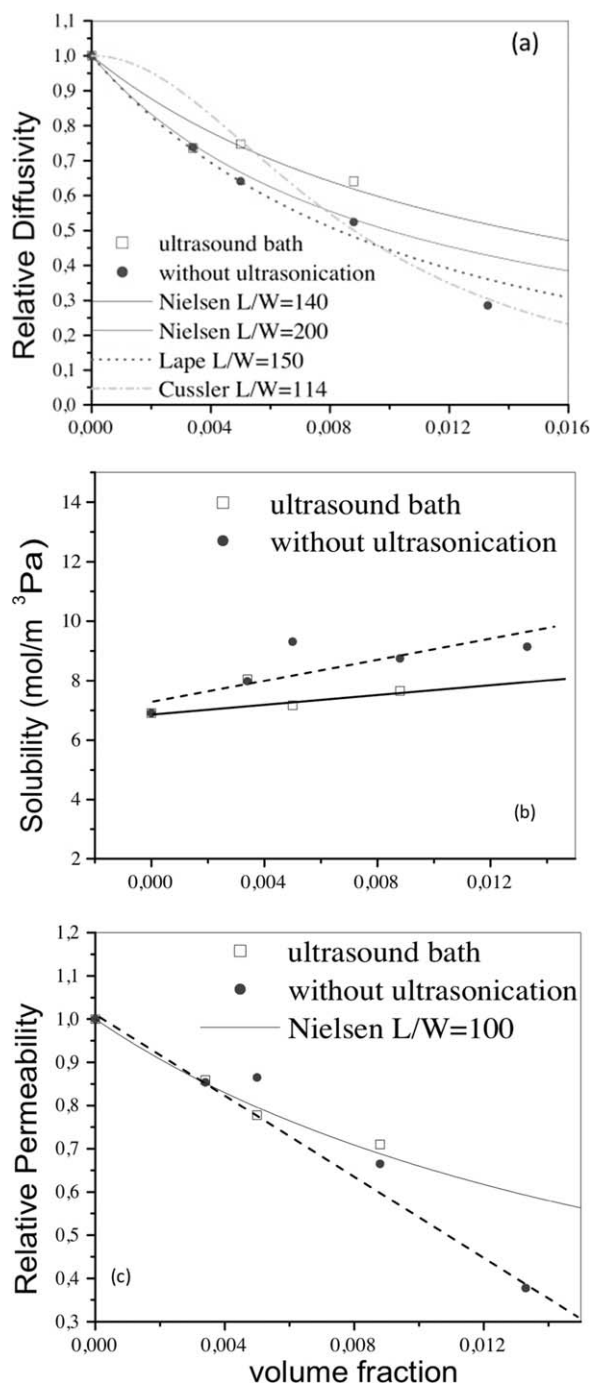
Figure 6. Transport coefficients for the acrylic resin/hectorite nanocomposite samples treated for 30 min in an ultrasound bath, or without any ultrasonic treatment, as a function of clay particles loading, at 23°C. (a) Relative diffusivity: Measurements and model predictions. (b) Solubility measurements; the lines are to guide the eye. (c) Relative permeability: The solid line gives the predictions of Nielsen's model for the "B" set of samples; the dashed line is to guide the eye for the "W" samples.

obtained [Figure 6(c)]. With less than 1 vol % reinforcement D is reduced by about 45%, S is increased by 25%, and P is reduced by about 30%. Nielsen's equation (eq. 7) can be fitted for this region (dilute region) and gives a value of the aspect ratio $\alpha \sim 200$. For higher volume fractions (semidilute region),

Nielsen's model fails to predict the reduction of D [Figure 6(a)], while Cussler's equation (eq. 8) seems to do a better job. The aspect ratio given by the latter is lower (114) than that of Nielsen's model. The total reduction of D is in the order of 70% with 1.3 vol % hectorite, while P is reduced only by 60% due to the negative impact of the solubility coefficient.

Figure 7 shows the results of the high-energy ultrasonicated samples. In the dilute region (<1 vol % clay) Nielsen's equation (eq. 4) is adequate to describe the diffusivity and gives a value for α of 300 [Figure 7(a)], significantly higher than the previous samples, due to better exfoliation. In this region S [Figure 7(b)] is significantly enhanced. In the semidilute region (above 1 vol %) Cussler's equation (eq. 8) is more suitable, the aspect ratio is predicted to be 105 and S remains almost constant. The relative permeability fits well Cussler's equation (eq. 7) in the whole range of volume fractions for $\alpha \sim 100$ [Figure 7(c)]. The overall reduction approaches an order of magnitude for 3.85 vol % hectorite, which is a significant improvement of the gas barrier properties of the membrane. Given their large aspect ratios, the barrier performance of these systems could be an order of magnitude better. It seems to be limited, however, by the defects introduced by spherical impurities, since the Li-hectorite particles may have such phase impurities.[22]

Validation of the Permeability Models
As it can be seen from Figures 6 and 7 Nielsen's model (eq. 4) underestimates the effectiveness of the tortuosity on the reduction of the diffusion coefficient in the semidilute region, while Cussler's model (eq. 8) deviates from the experimental results in the dilute region (< 1 vol %). On the other hand, Lape's model (eq. 10) seems to fit well both the dilute and the semidilute regions and gives averaged values for the aspect ratio of 150 [Figure 6(a)] and 180 [Figure 7(a)], respectively.

Nielsen's model describes very well the behavior of D in the dilute region, while Lape's model approaches Nielsen's model in the dilute region, and approximates Cussler's in the semidilute region. Lape's model can be considered as an average between the other two, resulting in a reliable approximation of the overall diffusion behavior.

The behavior of the relative permeability is described adequately by Cussler's equation (eq. 7) for $L/W \sim 100$. The Gusev-Lusti model (eq. 11) overestimates the barrier properties in the dilute region but coincides with Cussler's model at higher volume fractions (>3 vol %). Fitting the Gusev-Lusti [Figure 7(c)] equation gives exactly the same value for the aspect ratio ($L/W = 400$) as it was estimated by Möller et al.[12]

A reason for the aspect ratio predictions deviations among the models is the assumed shape of the particles. According to eq. 12 the aspect ratio for rectangular particles is equivalent to that of circular, which the Gusev-Lusti model considers, when multiplied with the factor $\sqrt{\pi} \approx 1.77$. Further, while macroscopically the permeation through the membrane is an 1D process, microscopically the diffusive jumps occur in 3D and the mobility of the gas molecule in the main direction depends on the mobilities in all directions. Thus, the barrier performance in 3D models requires higher values of α. This is the reason for the
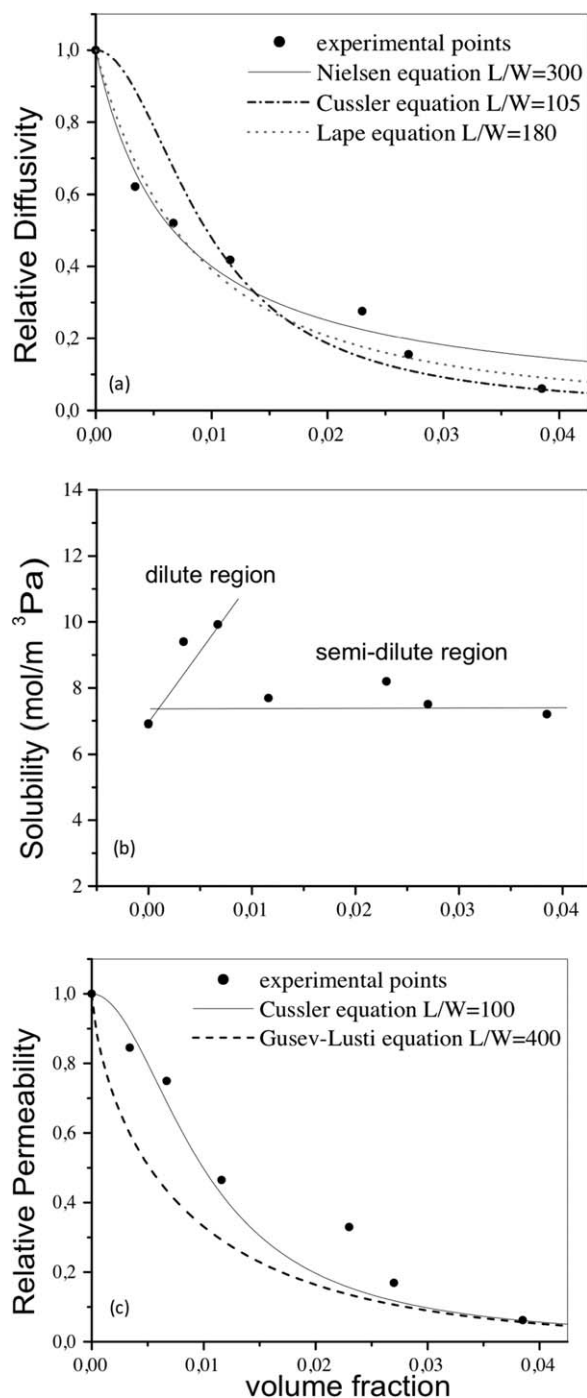
Figure 7. Transport coefficients at 23°C for the acrylic resin/hectorite nanocomposite samples treated with a high-energy ultrasonication probe, as a function of clay particles loading.

differences between predictions by the 2D Lape's eq. 9 and the 3D Gusev-Lusti models (eq. 11). This is probably the reason that the latter seems to better fit the relative permeability data in the semidilute region.

It seems, therefore, that the Cussler (eq. 7) and Gusev-Lusti (eq. 11) models are adequate to predict the relative permeability of the polymer/clay nanocomposites at high clay loadings but are less efficient for the low volume fractions region. The

differences in the values of α predicted by the two models arise from the assumption of periodic arrangement of the platelets in Cussler's model and random positions in Gusev-Lusti model. The aspect ratio should be higher in the latter case in order to give similar permeability results.

It should be noted, that the estimation of α by the models is more reliable if it is based on the relative diffusivity and not on permeability, since the impact of the solubility coefficient on the later may significantly alter the tortuosity effect and, consequently, the estimated value of α. Usually, the aspect ratio extracted from P is underestimated, as it is seen in the results of Figures 6 and 7.

The large reduction in relative permeability that Möller et al.[21] reported for nanocomposites with 11 vol % well-dispersed Li-hectorite in PU gives an estimated effective aspect ratio of ~410, based on the Gusev-Lusti model. Since the reduction in our sample of 3.85 vol % is about one order of magnitude, it seems logical that in water-based coatings with higher volume fractions of hectorite one should also expect similar reduction in permeability, i.e., two orders of magnitude or more.

Interfacial Region

Most permeability models are based on the assumption that the physical properties of the matrix (e.g., the free volume) do not change by the addition of the particles. This includes the solubility coefficient, which should remain constant or even slightly reduced in the nanocomposites (eq. 5). However, the experimental results of Figures 6(b) and 7(b) show that S_{comp} increases in the dilute region. This enhancement could be attributed to the adsorption of gas molecules in the interfacial regions developed between the matrix and the clay layers.

The interfacial region could have a thickness of some nm around the inorganic nanoparticles. The structure and dynamic properties in this region may be significantly different than those in the bulk polymer. The interactions between the two components (attractive, repulsive, or neutral), the width of the region, the density, the polymer chain mobility, and the free volume hole size distribution will influence the gas transport in the nanocomposite. For example, unfavorable interactions result in a disordered polymer structure, which leads to the formation of low-density layers adjacent to the nanoparticle surfaces. For large number of particles these layers occupy a considerable amount of volume and the permeability in the interfacial regions is expected to be higher than in the bulk. The interfacial regions may contain empty sites, which contribute to the free volume in the system, adding to the existing free volume in the matrix.

During the process of film formation, the inorganic layers are situated at the contact surfaces between the polar shells around the resin droplets. If the particles were not present, these shells would interact to each other and the droplets would coalesce, minimizing their contact area. However, the presence of the particles interrupts this minimization, forming particle/resin interfacial regions of significant lower density. Within the interfacial region, the polymer chains will be more mobile than in the bulk, since the T_g is significantly lower in the polar shell
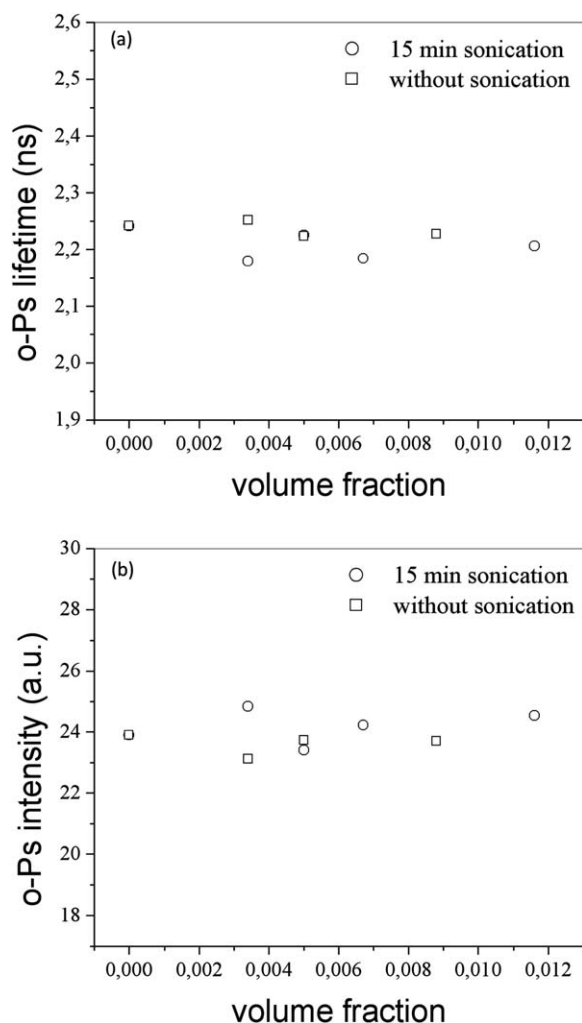
Figure 8. o-Ps lifetime, (a), and relative intensity, (b), for the acrylic resin/hectorite nanocomposite samples with (15 min) and without ultra-sonication treatment, as a function of hectorite volume fraction.

than in the nonpolar core. These effects influence the gas solubility coefficient.

The solubility trend [Figure 7(b)] can be divided in two regions. In the dilute region, where the interactions at the clay particles–resin interface are low, the interface density is low too, and the solubility increases. On the other hand, in the semidilute region, where the particles begin to overlap, these interactions become stronger, the interface is denser, and the solubility decreases (relative to the dilute region) and remains almost independent of the volume fraction.

In order to detect this extra free volume, positron annihilation lifetime measurements were performed. It was found that both the lifetime and the intensity of the o-Ps remained constant, independent of clay loading (Figure 8). It seems, therefore, that either this additional free volume is not generated or the PALS method cannot measure it. The latter could be attributed to presence of high charge on the hectorite particles surface, as there is no modifier to compensate it. The interfacial free volume becomes a strongly repulsive region for the positrons, which cannot be localized and annihilate in its holes. Therefore,

the PALS data may reflect only the contribution of the free volume inside the bulk of the amorphous matrix, which remains unchanged, since the particle volume fraction is very low.

To account for the surface charge, Xiao et al.[27] extended the Gusev-Lusti model to include a parameter, ε^{pn}, related to the polymer–nanoparticle interaction strength and the surface free energy of the components:

$$\frac{P_{comp}}{P_{matrix}} = \exp\left[-\left(\frac{\alpha\phi}{1.33}\right)^{0.68}\left(\frac{\varepsilon^{pn}}{1.72}\right)^{0.08}\right]. \quad (13)$$

The thickness of the interfacial region forming spontaneously between the resin and the particles should be proportional to this interaction strength.[28]

We tried to apply our data to eq. 13 but a single value for ε^{pn} could not give a good fit. It seems that the interaction strength between the two components is not constant and increases with clay loading. This is shown in Figure 9, where different fits were made at low, intermediate and higher volume fraction ranges. In the dilute region the interactions are weak and the interfacial areas have lower density and more free space, in agreement with the corresponding solubility results of Figure 7(b). For our system ε^{pn} takes a value of about $2 \cdot 10^{-5}$ then. As the particle volume fraction increases, the interfacial interaction becomes stronger and the solubility decreases. The values of ε^{pn} become about $5 \cdot 10^{-2}$ at intermediate and 5.7 at higher volume fractions.

There are still two questions to be answered with regard to mass transport through the nanocomposite: Why does the solubility significantly increase with the addition of clay in the dilute region? And why is the predicted aspect ratio relatively low, even for the exfoliated samples, when the actual surface of the hectorite particles is so large? A potential answer to the above questions is that the hectorite particles are flexible and may bend or crumble when dispersed in the polymer matrix. Tortuosity is a function mainly of the effective particle aspect
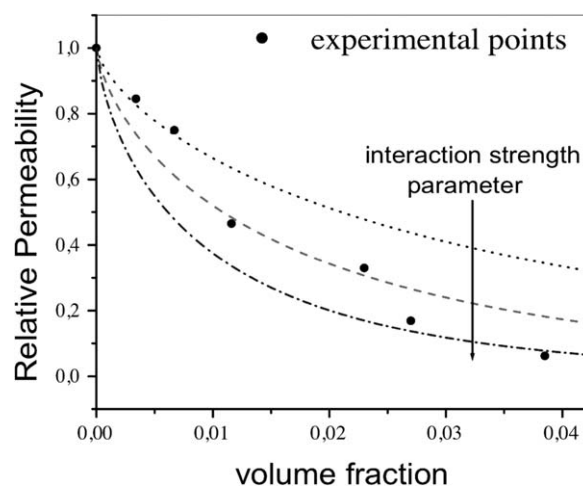
Figure 9. Fits of the permeability data using eq. 13, for an average aspect ratio of 107 and for three different values of the interaction strength parameter ε^{pn}, applicable in the different ranges of volume fractions.
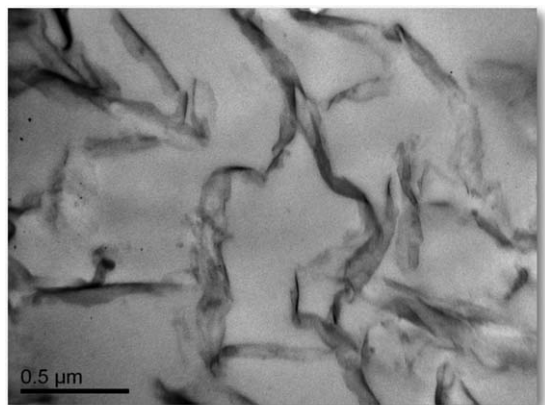
Figure 10. Transmission electron micrograph of nanocomposite sample U2 (0.67 vol % hectorite). The gray background corresponds to the resin. The lines and shadows are the projections of the clay particles (perpendicular to the thickness of the film). Notice that many hectorite particles are bent or crumbled.

ratio. The latter is based on the projection of the platelet on the plane perpendicular to the diffusion main direction. If parts of the platelets are not on this plane, e.g., due to bending or "crumbling," then the effective aspect ratio is lower than their primary aspect ratio and the tortuosity will be lower.

The flexibility of clay particles has been confirmed by Kunz et al.[29] and TEM observations by Osman et al.[30] A TEM image of sample 2U (Table I) is shown in Figure 10, where it can be seen that some clay particles may be crumbled in the nanocomposites of the present work. Entrapping of hydrophilic particles between the mainly hydrophobic polymer chains towards the end of the coating preparation process results in the development of capillary forces between the two components, which can deform the crystalline layers. The higher the degree of exfoliation, the higher the flexibility and the stronger the curvature. Under these circumstances, the effective aspect ratio of the particles may be significantly lower than their actual aspect ratio (Figure 11).

The degree of curvature of the particles will affect the area and the shape of the interfacial regions between the two components and, consequently, its accessibility by the gas molecules and the solubility coefficient. It seems that the higher the curvature and degree of exfoliation of the particles, the higher the increase of S. In combination with the results in Figure 9 this indicates that the bent (exfoliated) particles may present lower interactions with the polymer than the straight (less exfoliated) particles.

There is an additional experimental observation that supports the above arguments. The preparation of a coherent film was impossible when a high amount (above 4 wt %) of untreated hectorite particles were added to the resin, unless when ultrasonication was employed. This may also be related to the flexibility of the crystalline layers: The untreated particles are not fully exfoliated when their concentration exceeds a certain value. Thus, they are not flexible then, and they are unable to huddle on the template created by the resin's droplets.

Table II shows that the effect of the sonication treatment on the barrier properties is limited. Even in an aggregate form, the huge aspect ratio of the hectorite particles contributes significantly to the tortuosity. In fact, ultrasonication at high volume fractions serves mainly as a process to allow the incorporation of more clay in the resin. In this case, the tortuosity gets higher mainly due to the increased particle volume fraction, and not because of the higher aspect ratio, which is not improved in practice because of crumpling. Therefore, practically the overall
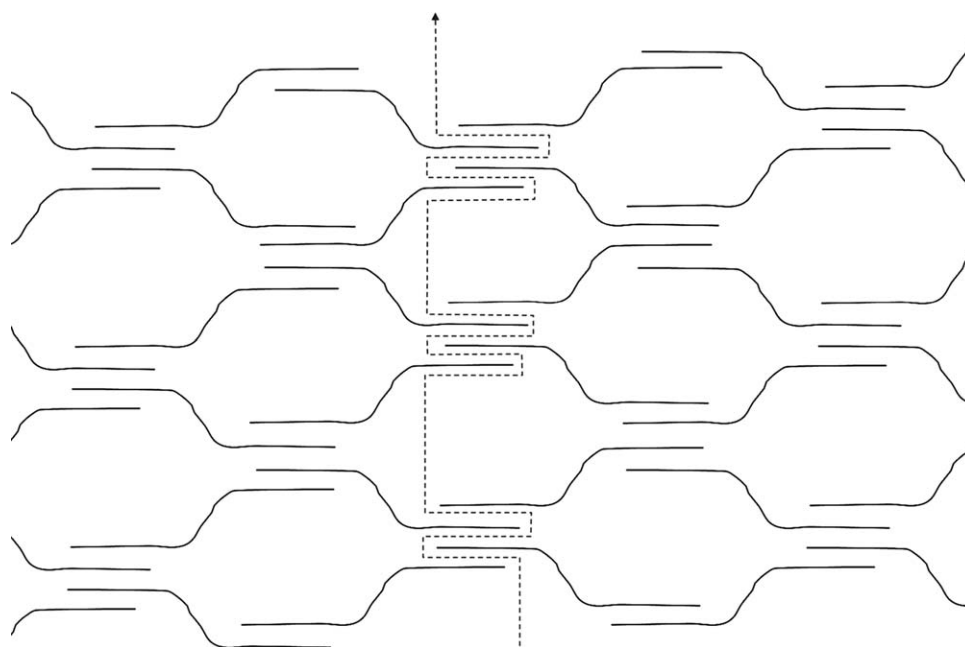
Figure 11. Schematic of periodical arrangement of curved nanolayers.[5] The effective aspect ratio of the particles is only a part of their actual aspect ratio. Note: stretching the layers will result in the picture in Figure 2.
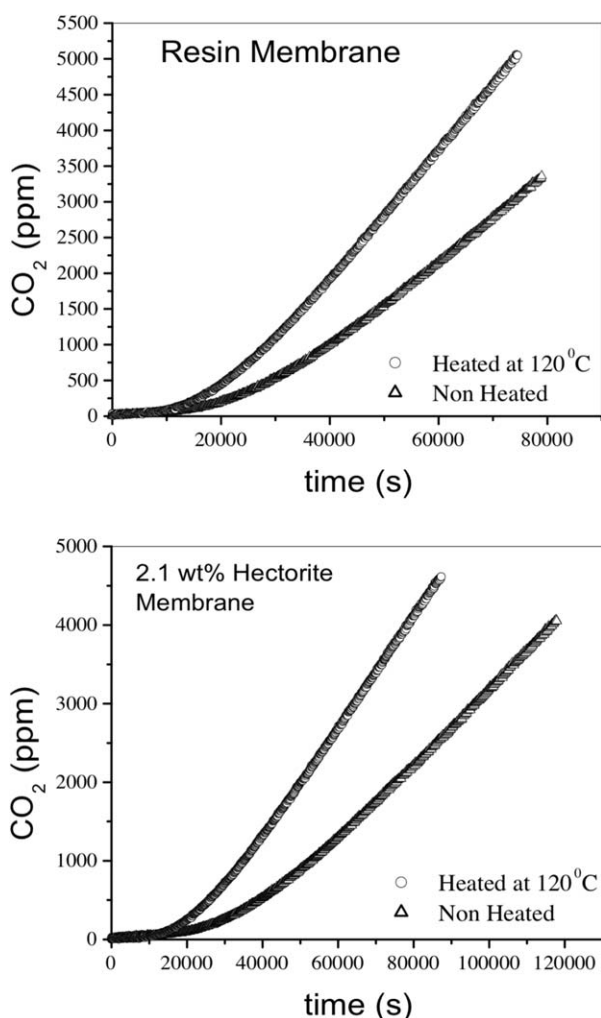
Figure 12. Permeation curves for two samples before and after heating at 120°C.

best barrier performance that was achieved in this work concerned the *U* samples.

Excess Free Volume

While the huge surface of the hectorite particles seems to be a remarkable advantage for their entrapping between the resin droplets during the preparation of the coating, as well as (mainly) for the exceptional improvement they evoke in the gas barrier properties, there are also some serious limitations. For coating applications using waterborne resins the volume fraction of the hectorite cannot be higher than 4 vol %. Otherwise, the viscosity of the suspension becomes unmanageable and the drying process of the film too slow, as the wide hectorite particles hinder water evaporation.

A significant amount of water could remain trapped inside the membrane even after the apparent completion of the drying process. The residual water molecules occupy an additional space, which would not have existed if the solvent had fully evaporated during the film formation process. In fact, this free space can be considered as an excess free volume. The higher the volume fraction of the nanoparticles, the higher the amount

of the entrapped solvent molecules, and the higher the excess free volume. This effect can limit the barrier performance of the nanocoating.

In order to check the influence of the trapped water molecules on the transport properties, two membranes were reheated above the glass transition temperature of the resin ($T_g = 120°C$) for 24 h and they were measured again in the permeation cell at 23°C. At $T > T_g$ the free volume is larger and the trapped water molecules have a chance to escape from the membrane. Depending on the chain dynamics and the crosslink density, the free volume created by escaping water molecules may be partly filled by macromolecular rearrangement or remain empty, increasing the total amount of free volume, which will affect the gas transport coefficients.

As it can be seen in Figure 12, both membranes show worse barrier properties after been heated at 120°C for 24 h: The weight loss of the membranes was 3–4%, while the gas barrier loss was about 45%. This reduction concerns mainly the diffusion coefficient and not the solubility, which remains almost constant.

Since membranes and films have lateral dimensions much larger than their thickness, most of the free volume is located near the surface and the amount of the free volume in the bulk is only a small part of the overall:

$$(\text{FFV})_t = (\text{FFV})_s + (\text{FFV})_b, \qquad (14)$$

where $(\text{FFV})_s$ and $(\text{FFV})_b$ are the fractional free volumes near the surface and in the bulk. The solubility coefficient is proportional to $(\text{FFV})_s$, while the diffusion coefficient has an exponential dependence on $(\text{FFV})_b$[13]:

$$D = \exp\left(-B/(\text{FFV})_b\right). \qquad (15)$$

The trapped water molecules are mainly located at the inner part of the membrane. When they diffuse away the generated new free volume will be mainly in the bulk. Thus, S will remain unchanged, while D will depend strongly on their removal. Even though the resulting change of the diffusion coefficient seems not to be as drastic as Möller et al.[12] expected, the permeation properties can be improved by almost an order of magnitude if the solvent/suspension medium is completely removed during the film formation process.

The full removal of the solvent can be achieved if the film formation process takes place at temperatures well above the T_g of the polymer. This could not be done in our case because the T_g of the acrylic resin was higher than the boiling point of the solvent. Thus, a coherent bubble-free membrane adequate for gas permeation experiments could not be made.

CONCLUSIONS

The incorporation of hydrophilic Li-Hectorite nanoparticles in acrylic resin matrix produces nanocomposite membranes with enhanced gas barrier properties. Because of their very large surface area, the hectorite particles create tortuous routes for the gas molecules increasing their diffusion length, even when they are not completely exfoliated. The overall reduction of the

relative permeability approaches an order of magnitude for volume fractions of less than 4%.

The experiments confirm that Nielsen's model describes the behavior of the relative diffusivity in the dilute region adequately, while Cussler's model is more appropriate to be used in the semidilute region. Lape's model seems to give intermediate predictions, with an average aspect ratio for both the dilute and the semidilute regions.

Because of the impact of the solubility coefficient, the relative permeability behavior is inadequate to predict reliable values of the aspect ratio of the clay particles, especially in the dilute region. In the semidilute region, however, where the solubility effect is less important, the Cussler or the Gusev-Lusti models for the relative permeability are appropriate.

During the film formation process, a significant amount of the solvent molecules may be trapped in the free volume sites of the polymer matrix. The subsequent removal of any residual solvent may generate additional free space (excess free volume), which could affect the gas diffusion and permeability coefficients by as high as 50%. The cure of this problem is the complete removal of the solvent during the film formation process. If this is not done, then the long term (slow) diffusion and evaporation of the water will manifest itself as a slow deterioration of the barrier properties of the coating (ageing) and will limit its useful lifetime.

The gas barrier performance of the Li-hectorite filled polymer coating would be even higher if the exfoliated crystalline layers remain flat and are not allowed to bend, maintaining, thus, their huge lateral dimensions. This would lead to the maximization of the tortuosity in the coating and could improve the gas barrier properties by one more orders of magnitude.

ACKNOWLEDGMENTS

REFERENCES

1. Louise Nobel, Water-borne nanocomposite coatings. PhD thesis, Delft University of Technology, Delft, the Netherlands, **2007**.

2. Jancar, J.; Douglas, J. F.; Starr, F. W.; Kumar, S. K.; Cassagnau, P.; Lesser, A. J.; Sternstein, S. S.; Buehler, M. *J. Polymer* **2010**, *51*, 3321.

3. Choudalakis, G.; Gotsis, A. D. In Handbook of Polymer Nanocomposites. Processing Performance and Application, Pandey, J. K.; Reddy, K. R.; Mohanty, A. K.; Misra, M. (Eds.), Springer, **2014**, ch. 11.

4. Choudalakis, G.; Gotsis, A. D. *Eur. Polym. J.* **2009**, *45*, 967.

5. Morris, G. E.; Zbik, M. S. *Int. J. Miner. Process* **2009**, *93*, 20.

6. Liang, Y.; Hilal, N.; Langston, P.; Starov, V. *Adv. Colloid Interface Sci.* **2007**, 134, 151.

7. Spalla, O. *Curr. Opin. Coll. Inter. Sci.* **2002**, *7*, 179.

8. Wicks, Z. W.; Jones, F. N.; Pappas, S. P.; Wicks, D. A. Organic Coatings: Science and Technology; John Wiley & Sons Inc.: Hoboken, New Jersey, **2007**.

9. Takahashi, S.; Goldberg, H. A.; Feeney, C. A.; Karim, D. P.; Farrell, M.; O'Leary, K.; Paul, D. R. *Polymer* **2006**, *47*, 3083.

10. Sun, Q.; Schork, F. J.; Deng, Y. *Comp. Sci. Tech.* **2007**, *67*, 1823.

11. Dai, C. F.; Li, P. R.; Yeh, J. M. *Eur. Polym. J.* **2008**, *44*, 2439.

12. Möller, M. W.; Lunkenbein, T.; Kalo, H.; Schieder, M.; Kunz, D. A.; Breu, J. *Adv. Mater.* **2010**, *22*, 5245.

13. Choudalakis, G.; Gotsis, A. D. *Curr. Opin. Coll. Inter. Sci.* **2012**, *17*, 132.

14. Choudalakis, G.; Gotsis, A. D.; Schut, H.; Picken, S. *J. Eur.Polym.J.* **2011**, *47*, 264.

15. Alexandre, B.; Colasse, L.; Langevin, D.; Mederic, P.; Aubry, T.; Chappey, C.; Marais, S. *J. Phys. Chem. B*, **2010**, *114*, 8827.

16. Alexandre, B.; Langevin, D.; Mederic, P.; Aubry, T.; Couderc, H.; Nguyen, Q. T.; Saiter, A.; Marais, S. *J. Membr. Sci.* **2009**, *328*, 186.

17. Herrera-Alonso, J. M.; Sedlakova, Z.; Marand, E. *J. Membr. Sci.* **2010**, *349*, 251.

18. Qian, Y.; Lindsay, C. I.; Macosko, C.; Stein, A. *ACS Appl. Mater. Interfaces*, **2011**, *3*, 3709.

19. Nielsen, L. E. *J. Macromol. Sci. A* **1967**, *1*, 929.

20. Cussler, E. L.; Hughes, S. E.; Ward, W. J.; Aris, R. *J. Membr. Sci.* **1988**, *38*, 161.

21. Möller, M. W.; Kunz, D. A.; Lunkenbein, T.; Sommer, S.; Nennemann, A.; Breu, J. *Adv. Mater.* **2012**, *24*, 2142.

22. Kalo, H.; Möller, M. W.; Kunz, D. A.; Breu, J. *Nanoscale* **2012**, *4*, 5633.

23. Russel, W. B. *AIChE J.* **2011**, *57*, 1378.

24. Pethrick, R. *Prog. Polym. Sci.* **1997**, *22*, 1.

25. Lape, N. K.; Nuxoll, E. E.; Cussler, E. L. *J. Membr. Sci.* **2004**, *236*, 29.

26. Gusev, A. A.; Lusti, H. R. *Adv. Mater.* **2001**, *13*(21), 1641.

27. Xiao, J.; Huang, Y.; Manke, C. W. *Ind. Eng. Chem. Res.* **2010**, *49*, 7718.

28. Grillet, C.; Brunel, A. S.; Chevalier, Y.; Usoni, S.; Ansanay-Alex, V.; Allemand, J. *Polym. Int.* **2004**, *53*, 569.

29. Kunz, D. A.; Max, E.; Weinkamer, R.; Lunkenbein, T.; Breu, J.; Fery, A. *Small* **2009**, *5*, 1816.

30. Osman, M. A.; Mittal, V.; Morbidelli, M.; Suter, U. W. *Macromolecules* **2003**, *36*, 9851.

31. Kalo, H.; Milius, W.; Breu, J. *RSC Adv.* **2012**, *2*, 8452.